Using Frequent, High-Resolution Remote Sensing to Identify Intermittent and Overlapping CH_4 sources in Oil and Gas Development Regions

M. J. Alvarado[1], A. Dayalu[1], D. B. Hogan[1], I. N. Polonsky[1], G. Start[2], P. Father[2], S. Aminfard[3], F. J. Cardoso-Saldaña[3], and C. A. Randles[4,5]

[1]Verisk Atmospheric and Environmental Research, Lexington, MA.

[2]Scepter, San Francisco, CA.

[3]ExxonMobil Technology and Engineering, Houston, TX.

[4]ExxonMobil Research and Engineering, Annandale, NJ.

[5]Now at United Nations Environment Program's International Methane Emissions Observatory, Paris, France.

Corresponding author: Matthew J. Alvarado (malvarad@aer.com)

Key Points:

- Quantifying CH_4 point source emissions as small as 50 kg hr^{-1} requires a ground resolution of 30-60 m and a column precision of 0.5-1.0%.
- Detecting intermittent sources with the above specifications is possible if the puff is observed within 15 min of emission.
- Plumes of similar source strengths within less than 0.5 km of each other will be difficult to separate in remote sensing observations.

Abstract

The oil and natural gas industry needs accurate and frequent information on methane CH_4 emissions from all of their facilities globally in order to effectively reduce emissions. Here we describe the development of requirements for a constellation of satellites to provide frequent data on point source CH_4 emissions from the oil and gas industry. Three types of sources were examined: isolated continuous plumes with emissions rates of 50 kg hr^{-1}, intermittent CH_4 releases from activities such as compressor start-ups, and overlapping continuous plumes. The dispersion model SCICHEM was used to simulate the dispersion of methane plumes and intermittent releases for typical meteorology in the Permian Basin, and a plume mask and integrated mass enhancement (IME) algorithm were applied to identify and quantify the emissions. The precision and ground sampling distance of the future satellite instrument were varied to determine the required precision and horizontal resolution of the satellite instrument. We find that quantifying CH_4 point source emissions as small as 50 kg hr^{-1} by remote sensing requires a ground sampling distance of 30-60 m and a CH_4 column precision of 0.5-1.0% for the range of conditions analyzed. Detecting intermittent sources is also possible with the above instrument specifications if the puff is observed within 15 min of emission. Plumes of similar source strengths more than 0.5 km apart can be separated with existing plume identification approaches but separating sources closer than that or with very different emission rates will require further development of plume identification techniques.

Plain Language Summary

In order to reduce greenhouse gas emissions from the oil and natural gas industry, and thus reduce near-term global warming, more frequent and accurate information on which of their facilities are emitting methane is needed. Satellite observations can help due to their global coverage, and recent advancements in sensor technology will make it possible to measure up to 80-90% of the methane emissions from the oil and gas industry. In this work we discuss instrument requirements toward a future group of satellites that will measure methane emissions from oil and gas facilities multiple times a day. We looked at small, steady sources of methane and determined that measuring these sources would require a satellite instrument that can measure methane to within 0.5-1.0% every 30-60 m horizontally. We find that detecting small, unsteady sources, such as those from starting a natural gas compressor, is also possible, but only if the source is observed within 15 minutes after the emission. Finally, we show that current techniques can only separate neighboring sources of CH_4 if they are of similar size and at least 0.5 km apart.

1 Introduction

Emissions of methane (CH_4) to the atmosphere are receiving increased attention as a method to reduce greenhouse gas radiative forcing and the resulting climatic changes (e.g., Nisbet et al., 2020). Reductions of CH_4 emissions are attractive as the relatively short lifetime of CH_4 in the atmosphere (9.1 ± 0.9 yr., Szopa et al., 2021) means that changes in CH_4 emissions could reduce climate forcing over a 10- to 20-year horizon, delaying when a given temperature threshold will be crossed and allowing for more time to address emissions of the longer-lived greenhouse gas carbon dioxide (CO_2).

CH_4 emissions come from a wide variety of sources, including natural sources such as wetlands and wildfires and anthropogenic sources like livestock, rice cultivation, landfills,

biofuel burning, and fossil fuel use (e.g., Saunois et al., 2020). Fossil fuel sources of CH_4 account for about 18% of the annual global CH_4 emissions and include emissions from coal mining (33% of fossil fuel CH_4 emissions for 2017) and the oil and natural gas industry (62% of fossil fuel CH_4 emissions for 2017, Saunois et al., 2020).

Emissions from oil and gas activities are complex as they are skewed, with a small number of sources accounting for a large fraction of emissions (Brandt et al., 2016), and have spatiotemporal variability (Allen et al., 2017; Cusworth et al, 2021). In recent years, high CH_4 emissions from oil and gas activities have been observed with aircraft and satellites in the US and around the world (Cusworth et al., 2021; Cusworth et al., 2022; Lauvaux et al. 2021), and they account for a disproportionate fraction of total emissions in a given region. For example, in the Permian basin, close to 90% of total emissions originate from plumes larger than 50 kg/hr (Chen et al., 2022). In order to achieve significant reductions on emissions, industry needs emission information in near-real-time for high emitter sources, such that mitigation measures can be taken to address unexpected CH_4 emissions when they appear (Cardoso-Saldaña 2022). In addition, the locations of emission sources need to be identified accurately to allow mitigation activities to be performed, especially as different companies may have emitting equipment within close proximity to each other. Finally, there is a need to detect intermittent sources of CH_4, as persistent emission sources account for only 29% of oil and natural gas industry emissions in areas like the Permian basin (Cusworth et al., 2021).

Providing the information on CH_4 emissions needed by the oil and gas industry will require a mixture of measurement approaches that combines in situ methane observations with additional information from ground-based (e.g., Pernini et al., 2022), aircraft (Duren et al., 2019; Jongaramrungruang et al., 2019; Cusworth et al., 2020), and satellite remote sensing platforms. Of these platforms, satellite observations are of particular interest due to their ability to observe methane sources globally.

Jacob et al. (2022) recently reviewed satellite methods to quantify methane emissions from the global scale down to individual point sources. They separated methane monitoring satellites into two general categories, area flux mappers and point source imagers. Area flux mappers are designed to observe total emissions on global or regional scales with 0.1–10 km pixel size (Jacob et al., 2022). These include the European Space Agency TROPOspheric Monitoring Instrument (TROPOMI) instrument, which has been used to detect high-emitting CH_4 sources in oil and gas fields with a low density of sites (Cusworth et al., 2018). Varon et al. (2022) created user-friendly, cloud-based facility for quantifying CH_4 emissions with $0.25^\circ \times 0.3125^\circ$ resolution by inverse analysis of satellite observations from TropOMI.

Point source imagers are fine-pixel (< 60 m) instruments designed to quantify individual point sources by imaging the plumes (Jacob et al., 2022). For example, Varon et al. (2020) used the GHGSat-D satellite instrument (50 m effective spatial resolution and 9–18% single-pass column precision) to quantify mean source rates for three coal mine vents (2320 to 5850 kg h^{-1}). Varon et al. (2021) used data from the Sentinel-2 mission to quantify point sources down to about 3 t h^{-1}, with Ehret et al. (2022) using similar methods to detect and quantify more than 1200 CH_4 emissions from Seninel-2 data. Sánchez-García et al. (2022) used data from the WorldView-3 (WV-3) satellite mission to detect point emissions over oil and gas extraction fields in Algeria and Turkmenistan.

The goal of the Scepter Monitoring Mission is to provide frequent, high-resolution data on multiple air pollutants to a variety of industrial and government entities. Here we focus on the development of requirements for a constellation of satellites to provide frequent data on point source CH_4 emissions from the oil and gas industry. A systems engineering requirement flow-down process was used to determine the satellite and constellation (~14 satellites) requirements to measure CH_4 leak rates of 50 kg hr^{-1} multiple times a day, thereby meeting the needs of the oil and gas industry. In this paper, we describe the first step of this process, where the dispersion model SCICHEM was used to simulate the dispersion of methane plumes during a typical day in the Permian Basin. The CH_4 emission rates were fixed at 50 kg hr^{-1} for different wind speeds and meteorological conditions and the resulting column enhancements (g m^{-2}) were calculated. A noisy background of CH_4 was added to simulate the satellite observations. Then a plume mask and integrated mass enhancement (IME) algorithm based on the approach of Varon et al. (2018) was applied. The value of the noise and the ground sampling distance of the instrument were varied to determine the required precision and horizontal resolution of the satellite instrument.

In addition, this paper focuses on two challenging aspects of monitoring oil and natural gas industry CH_4 emissions from satellites. First, intermittent, unintentional CH_4 releases need to be detected and quantified. Cusworth et al. (2022) showed these intermittent sources accounted for nearly half of the total CH_4 point source budget for multiple basins in the United States. To study these sources, we performed instantaneous releases in SCICHEM and applied the plume identification method of Varon et al. (2018) to the resulting puffs.

Second, at oil and gas facilities the plumes from multiple sources may overlap, making it more difficult to separate their emissions. This is less of a challenge for scientific studies that aim at determining the total CH_4 emission in a given region, as in those studies an accurate total emission rate is more important than separating the emissions among the individual sources. However, for our goal of providing information to operators that allow them to quickly address emissions, separating the emissions from different sources is critical to send staff to the correct location, as well as to identify which company should respond when the facilities of different companies are near each other. To address this, we simulated different configurations of overlapping plumes with the SCICHEM model, applied our plume masking algorithm, and examined how difficult it would be to separate the plumes under different wind directions, source strengths, and inter-plume distances.

2 Methods

2.1 Satellite Instrument Performance

We assumed a future satellite instrument operating in the 2050-2400 μm band with a signal to noise ratio (SNR) between 100-150, a spectral resolution between 1- 5 nm, and a ground sampling distance between 30-120 m. These specifications are well within the limits of current technology. We calculated the expected variance (σ) reduction due to adding a measurement to a system described by a prior information following Rodgers (2000):

$$\sigma^{-1} = K^T \left(\frac{SNR}{y}\right)^2 K + S_a^{-1}$$

where y is the measured radiance, K is the Jacobian (sensitivity of the radiance to changes in the CH_4 profile), SNR is the signal to noise ratio, and S_a is the prior covariance matrix. The Jacobians were computed using LBLRTM v12.13 (Clough et al., 2005, Alvarado et al., 2013) based on the finite difference method using a surface albedo of 0.15, which is less than the 25th percentile of surface albedo values in the Permian basin year-round. As we are interested in detecting near-surface enhancements of CH_4, the prior covariance was calculated assuming that the 1-sigma uncertainty in the CH_4 concentration in the planetary boundary layer was about 10% of the total column.

For an instrument with a SNR between 100-150 and a spectral resolution between 1- 5 nm, the above procedure estimated a CH_4 column precision of between 0.3-1.0%. However, this procedure does not account for the potential impacts of errors in other retrieved species (mainly H_2O and surface reflectance) on the retrieved CH_4 precision. Thus, for the plume identification and quantification studies below, we assumed a more conservative error range of 0.5-1.0%.

2.2 SCICHEM Dispersion Modeling

We used the SCICHEM dispersion model to simulate both continuous and instantaneous releases of CH_4. Hourly surface meteorological data were obtained from the Pine Springs, Guadalupe Mountains National Park (KGDP) weather station (31.83 °N, 104.81 °W) and upper air meteorological data was obtained from the Midland, TX station (WBAN 23023, 31.93 °N, 102.2 °W). The SCICHEM preprocessor METSCI was used to prepare the meteorological inputs, with the terrain preprocessor TERSCI used to simulate the terrain based on digital elevation model (DEM) data. Concentrations were calculated within a horizontal domain of 1 km with a spatial resolution of 30 m, and a vertical domain between 0-3 km agl at a vertical resolution of 25 m in the lowest 1 km and a 1 km resolution above. We determined the vertical resolution through initial SCICHEM runs (not shown) that demonstrated that the non-buoyant CH_4 emissions examined here rarely extended above 1 km in altitude before leaving the 1 km horizontal domain, but that a vertical resolution of greater than 25 m in the lowest 1 km led to > 0.1% errors in the calculated CH_4 column. We assumed a stack temperature of 30 ^{o}C and a stack exit velocity of 0.5 m s^{-1}, giving the plumes negligible buoyancy. CH_4 emissions from flares and compressor exhaust can be buoyant, but since the satellite measures vertically integrated CH_4 columns we expect the effects of buoyancy on our results to be minimal. We also expect most sources to be

near the surface, so the release height and release diameter were both set to 1 m. The CH_4 column enhancement was calculated as the vertical integral of the resulting CH_4 profiles.

Continuous release simulations were performed in the Permian for a number of different wind speeds. Our simulations covered one day (March 8, 2016) with a constant release rate of 50 kg hr^{-1}. We simulated a release at 32.065984 °N, -103.93936 °W, which is the location of Plume ID P00203 from the JPL Methane Plume Finder. SCICHEM was also used to simulate an instantaneous (<< 1 min) release of 33.5 kg of CH_4 at this location and date. The total emissions are roughly the median amount for a compressor blow-down and on the lower end of the range for a compressor start-up (Zimmerle et al., 2022) or liquid unloadings (e.g., Allen et al., 2015).

2.3 Plume Identification and Quantification

Our approach for identifying CH_4 plumes and quantifying CH_4 emission rates followed the integrated mass enhancement (IME) approach of Varon et al. (2018). The SCICHEM simulated column enhancement (Figure 1b) was added to a constant CH_4 background with 0.5% or 1% Gaussian noise applied (Figure 1c). The mean background column was set to 13.3 g m^{-2}, consistent with a background surface concentration of 2000 ppbv. The background CH_4 column distribution was then estimated using the up-wind quadrant of the 1 km modeling domain (Figure 1a).

The plume identification algorithm starts by performing a t-test to determine if the distribution of CH_4 columns in the 5x5 neighborhood of pixels around a given pixel is significantly different (95% confidence) from the background distribution. If so, the center pixel is tentatively marked as a plume pixel (Figure 1d). A median 3x3 filter is then applied to the resulting t-test mask to remove isolated pixels (Figure 1e), and then a Gaussian filter is applied to further remove spurious plume pixels (Figure 1f).

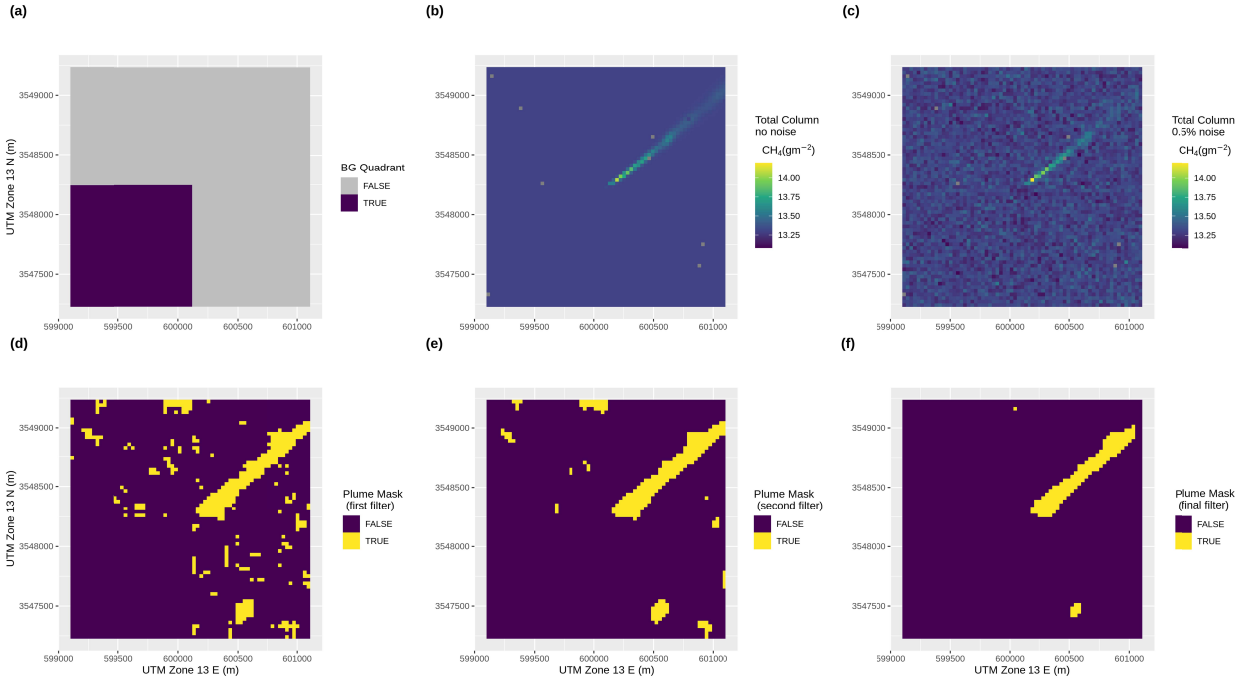

Figure 1. (a) Quadrant used to calculate mean and standard deviation of the background distribution. (b) Simulated plume from a point source of CH_4 with an emission rate of 50 kg hr^{-1}. (c) Addition of noisy background (13.3 g m^{-2} ± 0.5%). (d) Result of t-test plume identification. (e) Result of applying the median filter on (d). (f) Result of applying the Gaussian filter on (e).

Once the plume pixels have been identified, the *IME* (g CH_4) is defined as the area-weighted sum of the column enhancement of methane above background (Figure 2), following the equation

$$IME = \sum_{pixel=1}^{N_{pixel}} \left(\Omega_{CH4,pixel} - \Omega_b\right) A_{pixel} \quad (1)$$

where

- $\Omega_{CH4,pixel}$ is the measured methane column for a single pixel from the Level 2 product converted to units of g m^{-2}
- Ω_b is the background methane column in units of g m^{-2} estimated as discussed below
- A_{pixel} is the area of the pixel in units of m^2
- N_{pixel} is the number of pixels in a single plume

The IME is combined with the effective plume length:

$$L_{eff} = \sqrt{A_{plume}} = \sqrt{\sum_{pixel=1}^{Npixel} A_{pixel}} \quad (2)$$

and an effective wind speed U_{eff} (m/s) to estimate the emission rate (Q, g/s) via the equation:

$$Q = \frac{U_{eff}}{L_{eff}} IME \quad (3)$$

U_{eff} is calculated from the 10-m wind speed U_{10} using an equation of the form (Varon et al., 2018):

$$U_{eff} = a\, log U_{10} + b \quad (4)$$

Varon et al. (2018) used $a = 0.9$ and $b = 0.6$ m s^{-1}, and we use the same values for our continuous release tests.

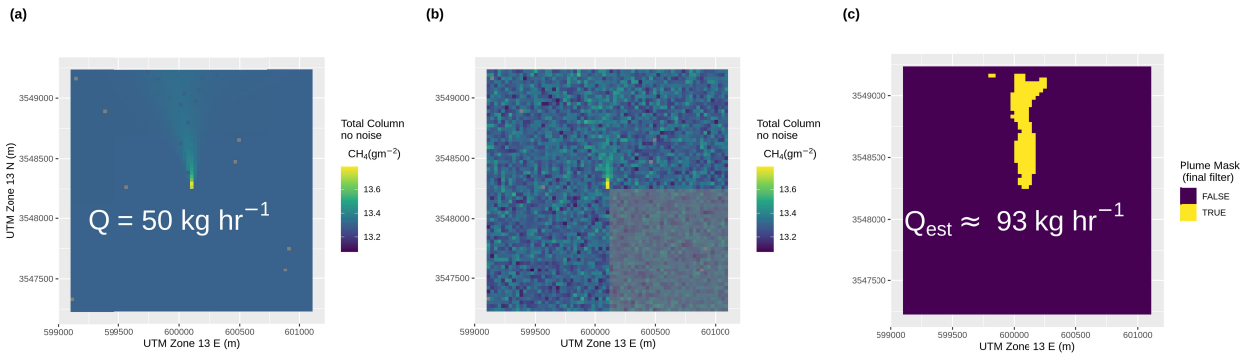

Figure 2. (a) Simulated plume from a point source of CH_4 with an emission rate of 50 kg hr^{-1} and U_{10} wind speed of 2.6 m s^{-1} at 16 UTC on March 8, 2016. (b) Addition of noisy background (13.3 g m^{-2} ± 0.5%). (c) Final plume mask and estimated emission rate.

2.4 Overlapping Continuous Sources

To simulate overlapping continuous sources, we took the simulation shown in Figure 2 and added a second source to the east at distances of 0.25, 0.5, and 0.75 km. The wind direction for the two plumes were rotated, such that a wind direction of 0^o simulated the wind being perpendicular to the line connecting the point sources and thus has the least overlap, while a wind direction of 90^o has the wind parallel to the line connecting the sources and thus has the most overlap. We also simulated the intermediate case of 45^o. Two cases were simulated for emission rates, one where both sources had an emission rate of 50 kg hr^{-1}, and one where the western source has a much larger release rate of 500 kg hr^{-1} while the eastern source remains at 50 kg hr^{-1}.

3 Results

3.1 Continuous Sources

Figure 2 shows the plume mask results for a fairly dispersive plume under low wind speed conditions (2.6 m s^{-1}) and an instrument precision of 0.5%. The plume mask for this case does identify the central core of the plume but is too conservative to identify the full extent of the plume. This suggests that there is room for improvement in the plume identification algorithm.

The retrieved emissions for the true 50 kg hr^{-1} rate vary between 25-200 kg hr^{-1} for the 24 hours (and thus 24 meteorological conditions) simulated. Figure 3 shows the mean estimated source rates for daytime hours (yellow bars), all hours (grey bars), and only hours with wind speed less than 5 m s^{-1} (blue bars) when 0.5% or 1.0% noise is added to the CH_4 background column. When data from all hours are averaged, the IME approach used here returns estimates with small positive biases (5-20 kg hr^{-1}). However, our assumed satellite instrument will only be able to make measurements in the daytime. Looking at only daytime hours leads to a positive bias of 25-50 kg hr^{-1}. The difference between the all-hours cases and the daylight-hours cases is that the all-hours cases include more cases with a stable atmosphere, suppressing vertical mixing.

Somewhat surprisingly, the higher noise case tends to have a lower positive bias. We believe this is a case of compensating errors: the positive bias comes from our U_{eff} parameterization, but the higher noise level leads to an underestimate of the plume extent, and thus IME, reducing the high noise bias.

The positive bias increases further (50-75 kg hr^{-1}) if only hours with wind speeds below 5 m s^{-1} are considered. As the plume mask tends to miss plume pixels, it is unlikely that the source of this bias is the plume mask or the IME calculation, which suggested that addressing these biases requires further refinement of the U_{eff} parameterization, potentially to include other meteorological inputs than just U_{10} wind speed.

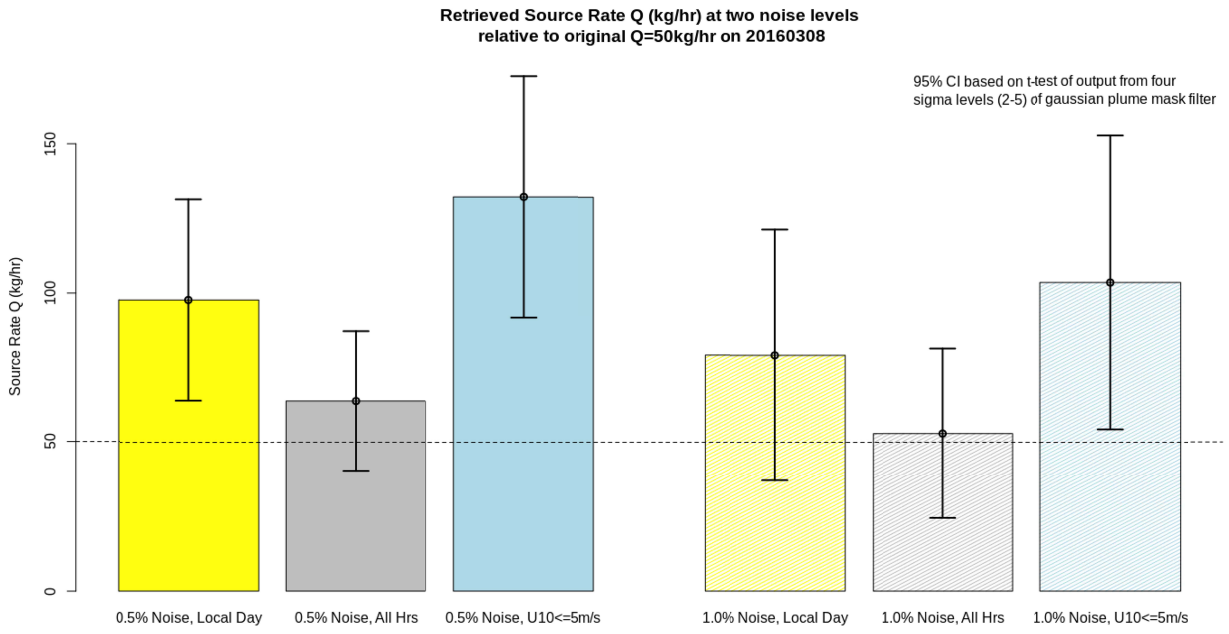

Figure 3. Mean and 95% confidence interval of the retrieved emission rates for the 50 kg hr-1 continuous releases. Solid bars (left) are for 0.5% Gaussian noise in the background, while the hatched bars (right) are for 1.0% Gaussian noise.

Figure 4 shows the plume simulation and masking results for a case with 4 m s^{-1} wind speed. The top row shows the results for the native 30 m horizontal resolution of the simulations, corresponding to a satellite ground sample distance of 30 m. We then degraded the resolution to 60 m, 90 m, and 120 m by averaging the original 30 m pixels and then applied the plume identification algorithm. Only at the 30 m resolution was the plume mask able to retain the shape of the simulated plume, with the other resolution only identifying enhanced blobs 0.25 – 0.75 km downwind from the original source. This again suggest that improvements are needed to the plume identification algorithm, as the plume can be clearly identified by eye at 60 m resolution, and somewhat at 90 m resolution. However, at 120 m resolution most of the plume enhancement has been lost in the background, suggesting that even an improved plume identification algorithm would not be able to identify a 50 kg hr^{-1} leak at this spatial resolution.

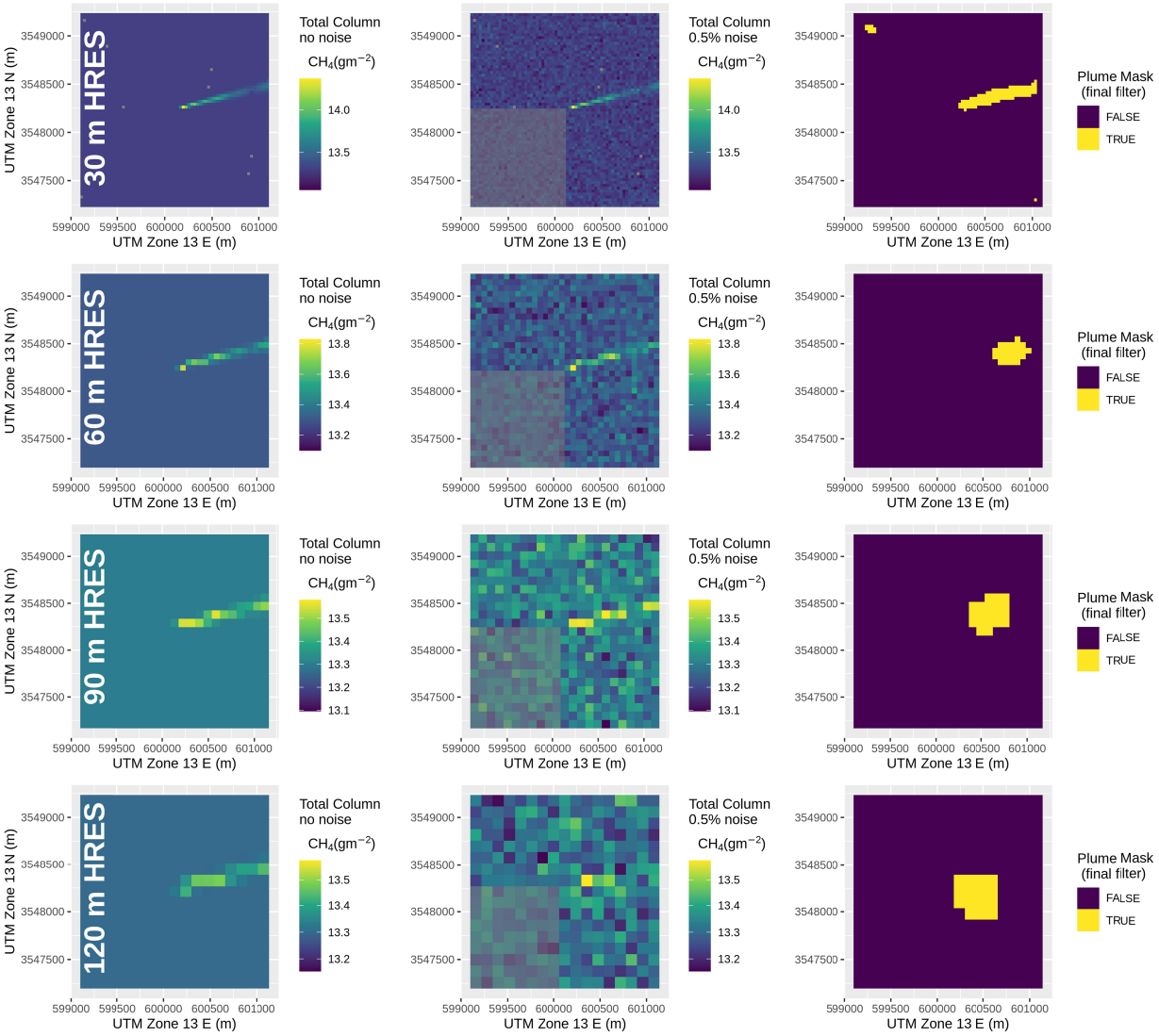

Figure 4. Impact of different horizontal resolutions on the plume identification algorithm. From top to bottom, the rows show the results at 30 m, 60 m, 90 m, and 120 m horizontal resolution. Left column is the simulated column enhancement for the plume, middle column is after a background with 0.5% noise is added, and right column is the resulting plume mask. All simulations are for a release rate of 50 kg hr^{-1} and a wind speed of 4.2 m s^{-1} (20 UTC on March 8, 2016).

3.2 Intermittent Sources

Figure 5 shows the results for the instantaneous release at 5 min (top row), 10 min (middle row) and 15 min (bottom row) after release for a 0.5% noisy background. The identification is very time dependent, as the instantaneous release results in a puff that is dispersing along both horizontal axes, resulting in concentrations that fall off more rapidly. The

maximum CH_4 column enhancement drops from 8 g m^{-2} at release start to 0.025 g m^{-2} 20 minutes downwind.

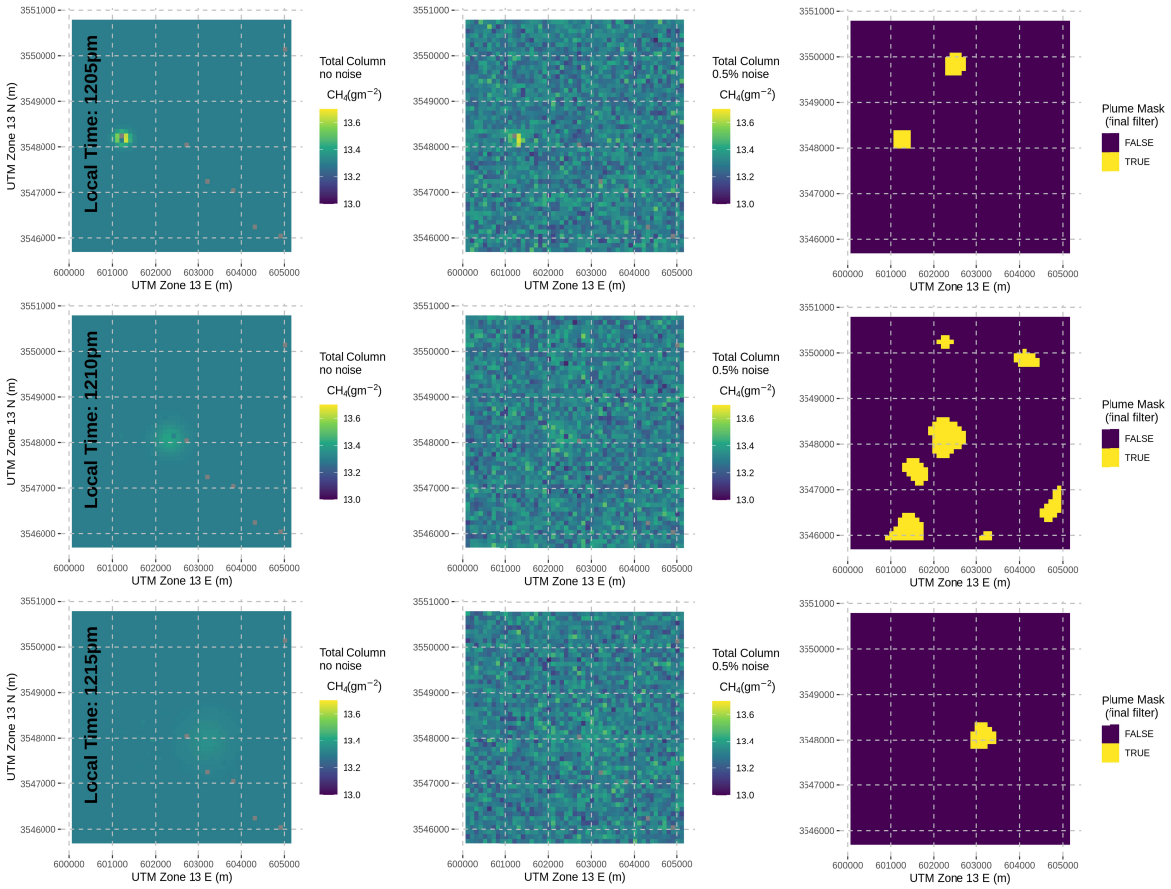

Figure 5. Plume identification results for an instantaneous release of 33.5 kg from a compressor blow-down at noon local time (UTC-7h) on March 8, 2016. From top to bottom, the rows show the results for 5, 10, and 15 minutes after emission. Left column is the simulated column enhancement for the plume, middle column is after a background with 0.5% noise is added, and right column is the resulting plume mask.

At 5 minutes, the puff is clearly identifiable by eye against the noisy background (Figure 5), and the plume identification algorithm successfully identifies the puff, although a spurious plume identification is also made to the northeast. At 10 min, it becomes difficult to identify the puff visually. While the plume identification algorithm does identify the puff location, it also classifies a large number of background locations as plume. At 15 min, it is difficult to identify the plume by eye, and the plume identification algorithm only identifies the central core of the plume, and after 15 min the puff is no longer detectable. This suggests an increased probability of detection of short duration events with higher frequency (hourly or less) observations.

3.3 Overlapping Continuous Sources

For cases with equal source strength of 50 kg hr^{-1} and a background column precision of

0.5%, the plume identification algorithm is generally able to separate the two overlapping sources if they are 0.5 km apart or more, regardless of the wind direction, but is not able to separate them if they are only 0.25 km apart. Figure 6 shows the most challenging case, where the wind is parallel with the line connecting the sources and so the upwind plume covers the downwind one (90-degree wind rotation from the original case in Figure 2). When the sources are only 0.25 km apart (top row), the plumes are merged in the plume mask. However, at 0.5 km (middle row) and 0.75 km (bottom row), the plume identification algorithm is able to distinguish the two plumes. Note that the horizontally dispersive case chosen here likely contributes to the ability to separate these plumes, as the centerline concentrations of the upwind plume have fallen to background levels before the second source is reached. Results for winds perpendicular to the line connecting the sources (zero-degree wind rotation) and the 45-degree rotation case, are shown in Supplemental Figures S1 and S2, respectively. The perpendicular shows two separate plumes when they are spaced 0.5 km and 0.75 km apart. At 0.25 km the two plumes merge into a single feature, with a small near-source bifurcation in the plume mask being the only indication of overlapping sources.

If the strength of the western source is increased to 500 kg hr^{-1}, the downwind plume is no longer separable from the upwind plume if the wind is parallel to the line connecting the sources (Supplemental Figure S3). This is true even if the locations of the sources are reversed

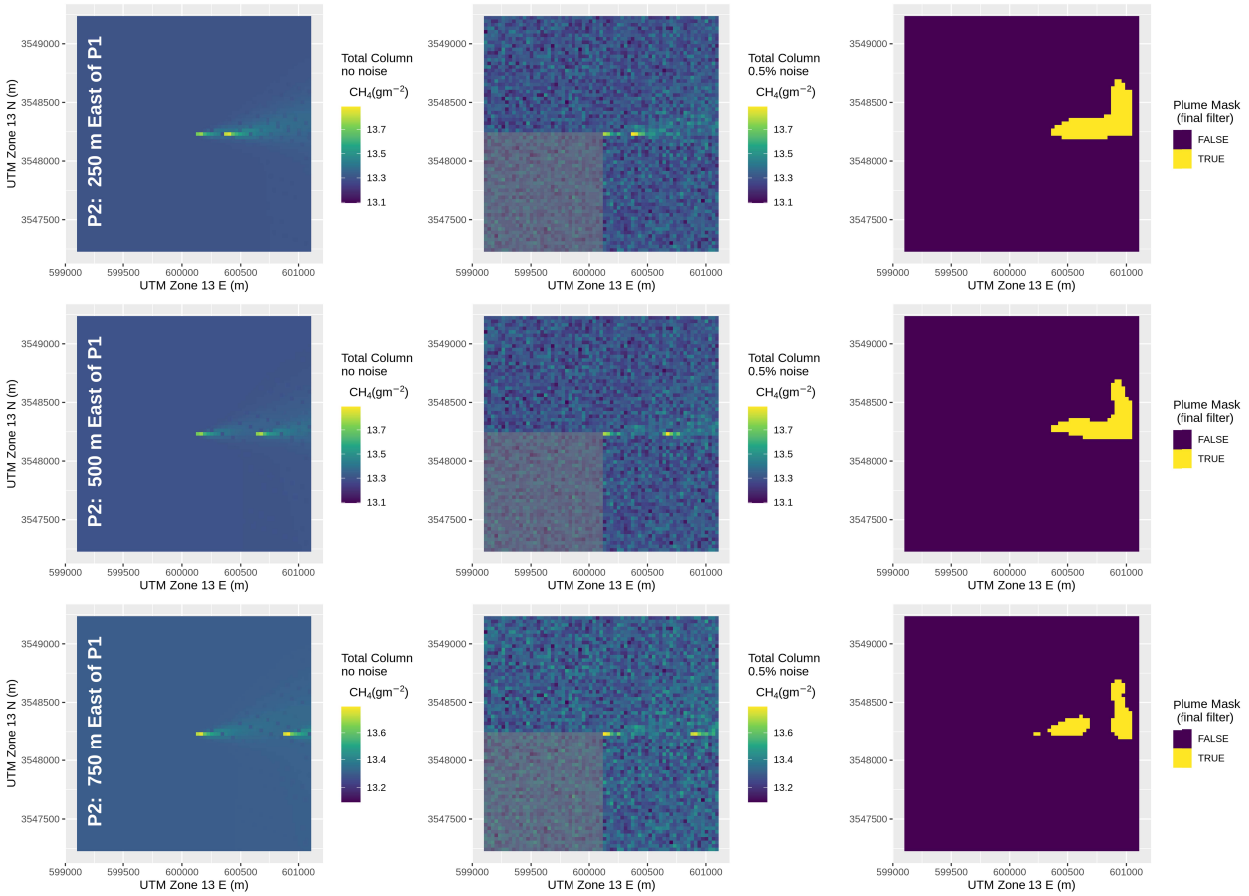

(not shown). Figure 7 shows the results if the wind is perpendicular. At 0.25 km, the second source is only identifiable as a small tendril disrupting the overall symmetry of the larger plume. At 0.5 km the tendril is more pronounced, and at 0.75 km we clearly see two distinct, if eventually overlapping, plumes. These plumes are in principle separable, but the plume identification algorithm would have to be refined to fully separate the two plumes. The 45-degree rotated case (Supplemental Figure S4) gives similar results to the perpendicular case in Figure 7.

Figure 6. Plume identification results for two sources emitting 50 kg hr^{-1} of CH_4 when the winds are parallel to the line connecting the two sources. From top to bottom, the rows show the results for when the sources are 0.25 km, 0.5 km, and 0.75 km apart. Left column is the simulated column enhancement for the plume, middle column is after a background with 0.5% noise is added, and right column is the resulting plume mask.

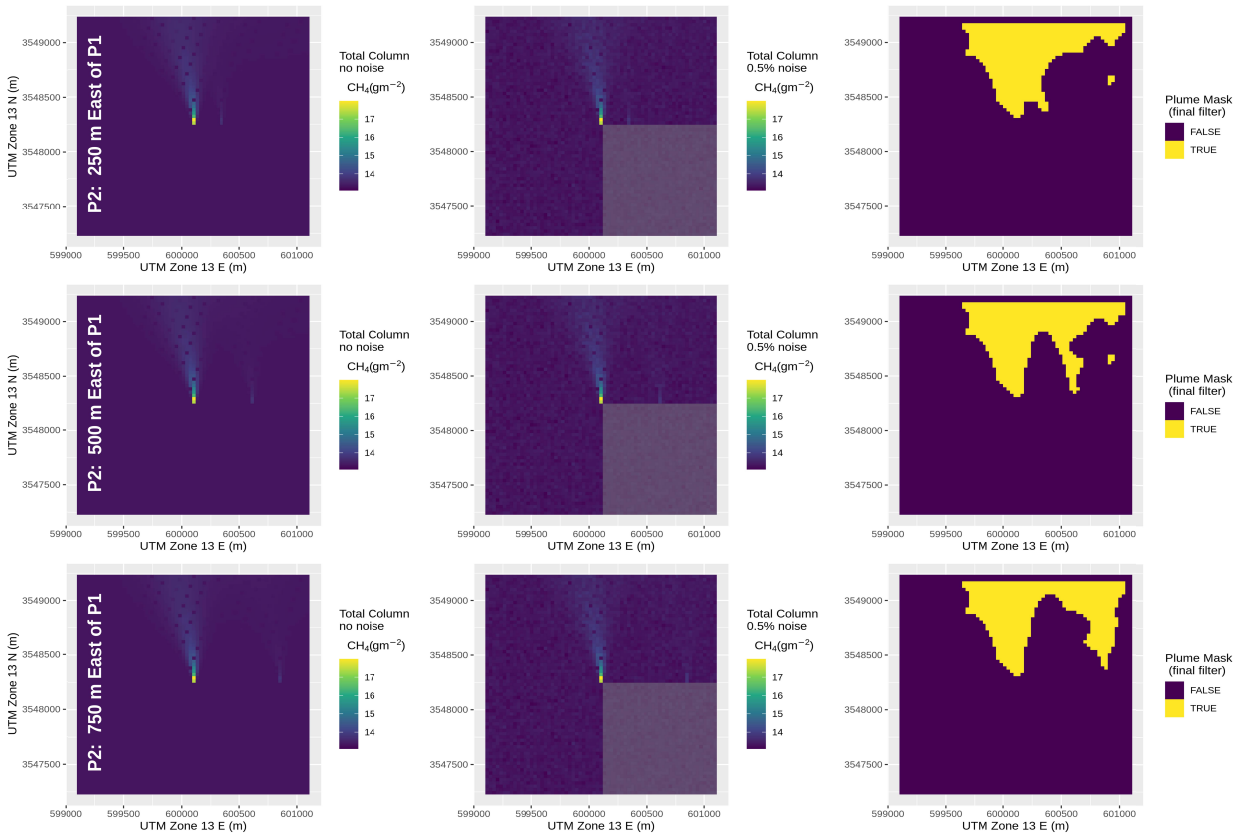

Figure 7. Plume identification results for two sources, the western one emitting 500 kg hr^{-1} of CH_4 and the eastern one emitting 50 kg hr^{-1} of CH_4 when the winds are perpendicular to the line connecting the two sources. From top to bottom, the rows show the results for when the sources are 0.25 km, 0.5 km, and 0.75 km apart. Left column is the simulated column enhancement for the plume, middle column is after a background with 0.5% noise is added, and right column is the resulting plume mask.

4 Conclusions

To help with the development of an operationally focused satellite constellation to detect CH_4 emissions for the oil and gas industry, we applied a plume identification and quantification method based on Varon et al. (2018) to three types of sources. First, isolated continuous sources with source strength of 50 kg hr^{-1} were simulated as 80-90% of methane sources from oil and gas are this size or larger. Second, an isolated instantaneous source of 33.5 kg was used to simulate an intermittent release from a compressor blowdown. Third, overlapping continuous sources were simulated for different distances, wind directions, and source strengths. A retrieved column precision of 0.5%-1.0% was assumed for these cases, based on a future satellite instrument operating in the 2050-2400 μm band with a signal to noise ratio (SNR) between 100-150 and a spectral resolution between 1- 5 nm.

For the isolated continuous sources, the retrieved emissions varied between 25-200 kg hr^{-1}, with the daytime cases showing a mean bias of 25-50 kg hr^{-1}. As the plume identification algorithm tends to be overly conservative in identifying pixels as within the plume, this positive

bias suggests the need for improvements in the U_{eff} parameterization used in the IME method. The plume mask performed the best at a horizontal resolution of 30-60 m, with the performance degrading significantly at horizontal resolution greater than 90 m.

As the instantaneous releases disperse in both horizontal directions, the CH_4 columns fall off as the square of distance/time downwind, rather than the linear decrease seen with continuous releases. This limits the time downwind that a puff from an instantaneous release is visible. With a 0.5% CH_4 column precision, a 33.5 kg CH_4 release is visible for 15 minutes after release. Thus, the typical compressor start-up, compressor blow-down, and liquid unloading with a plunger lift (7-200 kg, Allen et al., 2015) would have to be observed shortly after release to be detected by satellite. Liquid unloadings without plunger lifts tend to have larger releases (400-700 kg, Allen et al., 2015, Pacsi et al., 2020), and so may be visible for up to one hour after release. Thus, the releases larger than 50 kg/hr would be detected by satellite. Oil well completions tend to be a factor of 10 smaller (e.g., Cardoso-Saldaña and Allen, 2021), and so only the largest emitters would be detected.

Overlapping plumes of similar small source strength were difficult to separate if they were only 0.25 km apart but were separable by the plume identification algorithm if they were 0.5 km apart or more. This result was independent of whether the wind was perpendicular or parallel to the line connecting the two sources. However, when one source was much larger than the other, the resulting plumes tended to merge together downwind, although the sources were generally separable near the source. This suggests that a modified plume identification algorithm could be able to better separate these plumes.

Future work will focus on further refinement of the plume identification algorithm to better identify the full plume and to better separate overlapping plumes from neighboring sources. Further work is also needed to separate the puffs from intermittent sources from statistical fluctuations in the retrieved background columns. In addition, improvements in the parameterization of U_{eff}, potentially incorporating additional data beyond the U_{10} wind speed, should be explored.

Acknowledgments

Funding to perform the analyses reported here was provided by ExxonMobil Upstream Research Company.

Open Research

V3.3 of the SCICHEM model used for the dispersion modeling studies performed in this work is publicly available at https://github.com/epri-dev/SCICHEM/tree/3.3 from the Electric Power Research Institute. V12.13 of LBLRTM, used for calculating the Jacobians to estimate the precision of the retrieved methane columns for different assumptions of instrument resolution and SNR, is publicly available at https://github.com/AER-RC/LBLRTM from Verisk Atmospheric and Environmental Research. The LBLRTM license is free for all non-commercial research uses.

The input (meteorological and terrain) and output data (raw concentration output, calculated methane columns) from SCICHEM used in this study are available at zenodo via DOI 10.5281/zenodo.7757810 under a Creative Commons Attribution 4.0 International license.

References

Allen, D.T., Torres, V.M., Thomas, J., Sullivan, D.W., Harrison, M., Hendler, A., Herndon, S.C., Kolb, C.E., Fraser, M.P., Hill, A.D. & Lamb, B.K. (2013), Measurements of methane emissions at natural gas production sites in the United States. *Proceedings of the National Academy of Sciences, 110*(44), 17768-17773. https://doi.org/10.1073/pnas.130488011

Allen, D.T., Sullivan, D.W., Zavala-Araiza, D., Pacsi, A.P., Harrison, M., Keen, K., Fraser, M.P., Daniel Hill, A., Lamb, B.K., Sawyer, R.F. & Seinfeld, J.H. (2015), Methane emissions from process equipment at natural gas production sites in the United States: Liquid unloadings. *Environmental Science & Technology*, *49*(1), 641-648. https://doi.org/10.1021/es504016r

Allen, D.T., Cardoso-Saldaña, F.J. & Kimura, Y. (2017), Variability in spatially and temporally resolved emissions and hydrocarbon source fingerprints for oil and gas sources in shale gas production regions. *Environmental Science & Technology*, *51*(20), 12016-12026. https://doi.org/10.1021/acs.est.7b02202https://doi.org/10.1021/acs.est.7b02202

Alvarado, M.J., Payne, V.H., Mlawer, E.J., Uymin, G., Shephard, M.W., Cady-Pereira, K.E., Delamere, J.S. & Moncet, J.L. (2013), Performance of the Line-By-Line Radiative Transfer Model (LBLRTM) for temperature, water vapor, and trace gas retrievals: recent updates evaluated with IASI case studies. *Atmospheric Chemistry and Physics*, *13*(14), 6687-6711. https://doi.org/10.5194/acp-13-6687-2013

Brandt, A.R., Heath, G.A. & Cooley, D. (2016), Methane leaks from natural gas systems follow extreme distributions. *Environmental Science & Technology*, *50*(22), 12512-12520. http://dx.doi.org/10.1021/acs.est.6b04303

Cardoso-Saldaña, F.J. & Allen, D.T. (2021), Projecting the temporal evolution of methane emissions from oil and gas production basins. *Environmental Science & Technology*, *55*, 2811−2819. https://doi.org/10.1021/acs.est.0c04224

Cardoso-Saldaña, F.J. (2022), Tiered Leak Detection and Repair Programs at Oil and Gas Production Facilities. Preprint at chemrxiv.org, version 1. doi:10.26434/chemrxiv-2022-f7dfvdoi:10.26434/chemrxiv-2022-f7dfv

Chen, Y., Sherwin, E.D., Berman, E.S., Jones, B.B., Gordon, M.P., Wetherley, E.B., Kort, E.A. & Brandt, A.R. (2022), Quantifying Regional Methane Emissions in the New Mexico Permian Basin with a Comprehensive Aerial Survey. *Environmental Science & Technology*, *56*(7), 4317-4323. https://doi.org/10.1021/acs.est.1c06458

Clough, S.A., Shephard, M.W., Mlawer, E.J., Delamere, J.S., Iacono, M.J., Cady-Pereira, K., Boukabara, S. & Brown, P.D. (2005), Atmospheric radiative transfer modeling: A summary of the AER codes. *Journal of Quantitative Spectroscopy and Radiative Transfer*, *91*(2), 233-244. https://doi.org/10.1016/j.jqsrt.2004.05.058

Cusworth, D.H., Jacob, D.J., Sheng, J.X., Benmergui, J., Turner, A.J., Brandman, J., White, L. & Randles, C.A. (2018), Detecting high-emitting methane sources in oil/gas fields using satellite observations. *Atmospheric Chemistry and Physics, 18*(23), 16885-16896. https://doi.org/10.5194/acp-18-16885-2018

Cusworth, D.H., Jacob, D.J., Varon, D.J., Chan Miller, C., Liu, X., Chance, K., Thorpe, A.K., Duren, R.M., Miller, C.E., Thompson, D.R. & Frankenberg, C. (2019), Potential of next-generation imaging spectrometers to detect and quantify methane point sources from space. *Atmospheric Measurement Techniques*, *12*(10), 5655-5668. https://doi.org/10.5194/amt-12-5655-2019

Cusworth, D.H., Duren, R.M., Thorpe, A.K., Tseng, E., Thompson, D., Guha, A., Newman, S., Foster, K.T. & Miller, C.E. (2020), Using remote sensing to detect, validate, and quantify methane emissions from California solid waste operations. *Environmental Research Letters*, *15*(5), 054012. doi:10.1088/1748-9326/ab7b99

Cusworth, D.H., Duren, R.M., Thorpe, A.K., Olson-Duvall, W., Heckler, J., Chapman, J.W., Eastwood, M.L., Helmlinger, M.C., Green, R.O., Asner, G.P. & Dennison, P.E. (2021), Intermittency of large methane emitters in the Permian Basin. *Environmental Science & Technology Letters*, *8*(7), 567-573. https://doi.org/10.1021/acs.estlett.1c00173

Cusworth, D.H., Thorpe, A.K., Ayasse, A.K., Stepp, D., Heckler, J., Asner, G.P., Miller, C.E., Yadav, V., Chapman, J.W., Eastwood, M.L. & Green, R.O. (2022), Strong methane point sources contribute a disproportionate fraction of total emissions across multiple basins in the United States. *Proceedings of the National Academy of Sciences*, *119*(38), e2202338119. https://doi.org/10.1073/pnas.2202338119

Duren, R.M., Thorpe, A.K., Foster, K.T., Rafiq, T., Hopkins, F.M., Yadav, V., Bue, B.D., Thompson, D.R., Conley, S., Colombi, N.K. & Frankenberg, C. (2019), California's methane super-emitters. *Nature*, 575(7781), 180-184. https://doi.org/10.1038/s41586-019-1720-3

Ehret, T., De Truchis, A., Mazzolini, M., Morel, J.M., D'aspremont, A., Lauvaux, T., Duren, R., Cusworth, D. & Facciolo, G. (2022), Global tracking and quantification of oil and gas methane emissions from recurrent Sentinel-2 imagery. *Environmental Science & Technology*, *56*(14), 10517-10529. https://doi.org/10.1021/acs.est.1c08575

Jacob, D. J., Varon, D. J., Cusworth, D. H., Dennison, P. E., Frankenberg, C., Gautam, R., Guanter, L., Kelley, J., McKeever, J., Ott, L. E., Poulter, B., Qu, Z., Thorpe, A. K., Worden, J. R., & Duren, R. M. (2022), Quantifying methane emissions from the global scale down to point sources using satellite observations of atmospheric methane. *Atmospheric Chemistry and Physics, 22*, 9617–9646. https://doi.org/10.5194/acp-22-9617-2022

Jongaramrungruang, S., Frankenberg, C., Matheou, G., Thorpe, A.K., Thompson, D.R., Kuai, L. & Duren, R.M. (2019), Towards accurate methane point-source quantification from high-resolution 2-D plume imagery. *Atmospheric Measurement Techniques, 12*(12), 6667-6681. https://doi.org/10.5194/amt-12-6667-2019

Lauvaux, T., Giron, C., Mazzolini, M., d'Aspremont, A., Duren, R., Cusworth, D., Shindell, D. & Ciais, P. (2022), Global assessment of oil and gas methane ultra-emitters. *Science*, *375*(6580), 557-561. DOI: 10.1126/science.abj4351DOI: 10.1126/science.abj4351

Nisbet, E.G., Fisher, R.E., Lowry, D., France, J.L., Allen, G., Bakkaloglu, S., Broderick, T.J., Cain, M., Coleman, M., Fernandez, J. & Forster, G. (2020), Methane mitigation: methods to reduce emissions, on the path to the Paris agreement. *Reviews of Geophysics*, *58*(1), e2019RG000675. https://doi.org/10.1029/2019RG000675

Pacsi, A., Sullivan, D.W. & Allen, D.T. (2020), Revised Estimation Method for Emissions from Automated Plunger Lift Liquid Unloadings. *Environments*, *7*(4), 25. https://doi.org/10.3390/environments7040025

Pernini, T.G., Zaccheo, T.S., Dobler, J. & Blume, N. (2022), Estimating oil sands emissions using horizontal path-integrated column measurements. *Atmospheric Measurement Techniques, 15*(2), 225-240. https://doi.org/10.5194/amt-15-225-2022

Sánchez-García, E., Gorroño, J., Irakulis-Loitxate, I., Varon, D.J. & Guanter, L. (2022), Mapping methane plumes at very high spatial resolution with the WorldView-3 satellite. *Atmospheric Measurement Techniques*, *15*(6), 1657-1674. https://doi.org/10.5194/amt-15-1657-2022

Saunois, M., Stavert, A.R., Poulter, B., Bousquet, P., Canadell, J.G., Jackson, R.B., Raymond, P.A., Dlugokencky, E.J., Houweling, S., Patra, P.K. & Ciais, P. (2020), The global methane budget 2000–2017. *Earth System Science Data*, *12*(3), 1561-1623. https://doi.org/10.5194/essd-12-1561-2020

Szopa, S., V. Naik, B. Adhikary, P. Artaxo, T. Berntsen, W.D. Collins, S. Fuzzi, L. Gallardo, A. Kiendler-Scharr, Z. Klimont, H. Liao, N. Unger, & P. Zanis (2021), Short-Lived Climate Forcers. In *Climate Change 2021: The Physical Science Basis. Contribution of Working Group I to the Sixth Assessment Report of the Intergovernmental Panel on Climate Change* [Masson-Delmotte, V., P. Zhai, A. Pirani, S.L. Connors, C. Péan, S. Berger, N. Caud, Y. Chen, L. Goldfarb, M.I. Gomis, M. Huang, K. Leitzell, E. Lonnoy, J.B.R. Matthews, T.K. Maycock, T. Waterfield, O. Yelekçi, R. Yu, & B. Zhou (eds.)]. Cambridge University Press, Cambridge, United Kingdom and New York, NY, USA, 817–922. doi:10.1017/9781009157896.008

United States Environmental Protection Agency (2021), Standards of Performance for New, Reconstructed, and Modified Sources and Emissions dssdfgsdgf for Existing Sources: Oil and Natural Gas Sector Climate Review, 86 Fed. Reg. 63,110 (Nov. 15, 2021).

Varon, D.J., Jacob, D.J., McKeever, J., Jervis, D., Durak, B.O., Xia, Y. & Huang, Y. (2018), Quantifying methane point sources from fine-scale satellite observations of atmospheric methane plumes. *Atmospheric Measurement Techniques*, *11*(10), 5673-5686. https://doi.org/10.5194/amt-11-5673-2018

Varon, D.J., Jacob, D.J., Jervis, D. & McKeever, J. (2020), Quantifying time-averaged methane emissions from individual coal mine vents with GHGSat-D satellite observations. *Environmental Science & Technology*, *54*(16), 10246-10253. https://doi.org/10.1021/acs.est.0c01213

Varon, D.J., Jervis, D., McKeever, J., Spence, I., Gains, D. & Jacob, D.J. (2021), High-frequency monitoring of anomalous methane point sources with multispectral Sentinel-2 satellite observations. *Atmospheric Measurement Techniques*, *14*(4), 2771-2785. https://doi.org/10.5194/amt-14-2771-2021

Varon, D.J., Jacob, D.J., Sulprizio, M., Estrada, L.A., Downs, W.B., Shen, L., Hancock, S.E., Nesser, H., Qu, Z., Penn, E. & Chen, Z. (2022), Integrated Methane Inversion (IMI 1.0): a user-friendly, cloud-based facility for inferring high-resolution methane emissions from TROPOMI satellite observations. *Geoscientific Model Development*, *15*(14), 5787-5805. https://doi.org/10.5194/gmd-15-5787-2022

Zimmerle, D., Duggan, G., Vaughn, T., Bell, C., Lute, C., Bennett, K., Kimura, Y., Cardoso-Saldaña, F.J. & Allen, D.T. (2022), Modeling air emissions from complex facilities at detailed temporal and spatial resolution: The Methane Emission Estimation Tool (MEET). *Science of The Total Environment*, *824*, 153653. https://doi.org/10.1016/j.scitotenv.2022.153653